International Journal of
INTELLIGENT SYSTEMS AND APPLICATIONS IN ENGINEERING
ISSN:2147-6799 www.ijisae.org Original Research Paper

Covid-19 Detection by X-Ray Images Using Deep Residual Network with Optimize Segmentation

Sukhwinder Bir*[1], Dr. Vijay Dhir[2]

Submitted: 10/10/2023 **Revised**: 30/11/2023 **Accepted**: 10/12/2023

Abstract: For the purpose of COVID-19 lesion segmentation, the Covid-SegNet model has been suggested. The design of the UNet has been improved and is now known as the CovidSegNet. The receptive field of the encoder in the UNet is constantly restricted to a minimal size. As a result, the issue of a tiny receptive field is addressed with Covid-SegNet by the use of the atrous spatial pyramid pooling technique. down order to zero down on the fine-grained characteristics, the channel and spatial-wise attention processes are also used. In addition to this, the ablation research is carried out to emphasize the significance of these alterations to the UNet model. The ReSE- Net algorithm is suggested for use in the fourth research for the purpose of lung segmentation in chest x-rays. Additionally, it is the encoder-decoder architecture that is improved upon and based on UNet. It makes use of residual learning in both the encoder and the decoder, whereas the attention layer is implemented in the encoder in order to re-calibrate the features. The ReSE-Net algorithm is tested using three different chest x-ray datasets before being verified using a CT-scan dataset. In addition, ablation research is carried out in order to emphasize the influence that the attention mechanism has on the model that is being offered. In addition, a non-parametric statistical test is carried out to validate the findings' significant statistical relevance. In both the intra-dataset and cross-dataset evaluations, the performance of the suggested model was superior than that of the UNet model. In the fifth investigation, a method known as transfer learning is used for the purpose of lung segmentation. As an encoder, the suggested EfficientUNet model makes use of a modified version of the pre-trained EfficientNet-B4 network. In addition to this, an ablation study is carried out to illustrate the effects of the modifications made to the encoder and the decoder. In addition, when compared to the performance of the ReSE-Net model in the cross-dataset generalization test, the EfficientUNet model demonstrated superior results. The performance of EfficientUNet was superior to that of all the models suggested in similar research, including the design of UNet. Through illness identification and lung segmentation applications, this thesis demonstrates the promise of deep learning for chest x-ray interpretation.

Keywords: *CNN, X-ray Images, LSTM-RNN, Extreme Leaner, Machine Lerning, Covid-19*

1. Introduction

The COVID-19 virus has the ability to cause significant respiratory conditions, ranging from the common cold to fatal infections like Middle East Respiratory Syndrome (MERS) and severe acute respiratory syndrome (SARS). According to the World Health Organization (WHO), the most common symptoms of COVID-19 are the same as those of the dry cough, exhaustion, common flu: fever, aches, breathing problems, and throat pain. The fact that the signs and symp- toms of COVID-19 and influenza are identical complicates the early identification of coronavirus. It is known that the coronavirus along with other bacterial and viral infections may result in pneumonia in some persons. However, treatment for pneumonia caused by a coronavirus differs from the methods employed for other types of pneumonia. In addition, antibiotics are necessary for individuals infected with bacterial pneumonia, while intensive care is an option for patients infected with viral pneumonia [1] Therefore, an accurate and speedy diagnosis of pneumonia brought on by COVID -19 is necessary for preventing further loss of human life and bringing the pandemic under control. The World Health Organization [2] recommends the reverse transcription polymerase chain reaction (RT-PCR), wherein brief sequences of RNA are examined in order to test for COVID-19 and determine whether a coronavirus is present. Yet, the following difficulties may be encountered when attempting to detect COVID-19 employing current methods: (1) A lack of positive RT-PCR data does not rule out the likelihood of a COVID-19 infection. This necessitates more testing to exclude the likelihood of a false negative result [3], [4], [5] (2) Outbreak

[1] *Sant Baba Bhag Singh University, Punjab, India; sukhwinderbir@gmail.com;*
[2] *Sant Baba Bhag Singh University, Punjab, India; drvijaydhir@gmail.com*

hotspots in economically disadvantaged areas have additional challenges due to the scarcity of kits for testing and screen workstations. Additionally, the increased death risk from pneumonia caused by COVID-19 makes it all the more important to catch the virus early. The variable incubation period—the time between contracting the virus and developing symptoms—greatly re- duces the efficiency of early detection. This period can range from 1-14 days. These difficulties underline the importance of creating new methods for detecting COVID-19. Medical professionals typically rely on chest X-ray imaging to confirm or rule out the presence of pneumonia. Chronic obstructive pulmonary disease and Emphysema, both of which can be fatal, are associated with a rise in lung density, as was found in an earlier investigation [9,10]. A COVID-19 chest scan imaging includes significant imaging abnormalities, including white lines (horizontal), bands, or retinal alterations, as well as opacity in the ground glass [6], [7]. Chest X-ray images possess a chance to be used for surveillance and examination of lung conditions like infiltration, tuberculosis, atelectasis, hernia, and pneumonia. The detrimental effects of Covid- 19 on the lungs can be monitored by chest X-rays [8] In other words, thoracic X-ray images could be employed for recognizing Covid-19 [9] By looking for persistent visual alterations on a chest X-ray, this imaging technique can be em- ployed as a main screening tool for detecting COVID-19 [10]. While higher-resolution imaging techniques like computed tomography (CT) are available, chest X-ray images are both affordable and sensitive [11], [12] . Without readily available kits for testing and screen stations, the utilization of X-ray machinery as a means of COVID-19 detection emerges as an intriguing alternative. The manual inspection for every X-ray image and recovery of the information presents the greatest obstacle for an X-ray-based COVID-19 detection method. Ex-perts' participation and considerable time are needed for this. To determine COVID-19 cases, therefore, computer-assisted inspection of chest X-ray images is required. To this end, deep learning (DL) techniques [13], [14] have been effective in producing high-quality outputs, along with other benefits like (1) making the most of unstructured data; (2) cutting back on unnecessary expenditures; (3) cutting down on feature engineering; and (4) eliminating the need for identifying labels on data. Consequently, strategies of deep learning are frequently utilized to derive beneficial features for independently categorizing visual objects. Methods based on deep learning have made important contributions to the analysis of medical images, allowing for greater accuracy in classification with fewer resource-intensive simulated tasks [3]. Deep learning has recently supported a growing focus on studies and has surpassed several traditional models in performance [15], [16], [17], [18] Deep learning methods can efficiently pick up the features of CXR images while requiring fewer training cycles. It is a beneficial educational resource that addresses the intellectual and technical problems that arise during COVID-19 diagnosis. Convolutional neural networks (CNNs), one deep learning technique, however, need a lot of initial training data and may overfit with small amounts of data. Algorithms from deep learning may be used to extract pertinent results from medical data, it is anticipated. Deep learning's strengths include its ability to handle large and complex datasets, making it ideally suited for image processing. In addition, this method may lessen the possibility of overfitting and incorrect classifications [29]. Numerous studies have shown that massive amounts of data significantly improve CNNs' effectiveness. To develop deep learning networks, several pre- trained models [31-40] are available to choose from. These include GoogLeNet, LeNet, AlexNet, VGG19, VGG16, and Resnet50 [19]

Gaps in previous Work

COVID X-ray image classification is an important application of deep learning in healthcare. The goal is to use machine learning algorithms to classify chest X-ray images into two categories: COVID-19 positive or negative. This can help in the early detection of COVID-19 cases and can aid in the diagnosis of the disease.:

- The Literature highlights several challenges in the application of deep learning (DL) models for COVID-19 diagnosis using CXR/CT images. One of the key challenges is the limited availability of annotated data, which can make it difficult to train accurate models [20]
- Another challenge is the high number of training parameters and memory requirements of DL models which can make them computationally expensive and difficult to deploy in resource-constrained settings [21], [22]

- The Literature highlights the importance of hyperparameter tuning in achieving optimal performance with DL models. There is a need for more research on different hyperparameters, such as learning rate, batch size, and optimizer type, to optimize performance for COVID-19 detection.
- The Literature also notes that most existing studies have focused on binary classification scenarios, and there is a need for more research on multi-class classification, which is more challenging but in high demand for COVID-19 diagnosis [19]

Overall, the Literature highlights the need for lightweight DL models with optimized hyper parameters and improved performance in multi-class classification scenarios to enable more accurate and reliable COVID-19 diagnosis using CXR images.

Contribution of Research

- In this paper Improve the non-linear features mapping by Deep learning approaches.
- Improve the learning of features by optimize extreme learner

The rest of this paper is structured as follows. Section 2 gives a review on the state-of-the-art deep Learning models as image classifiers. In third section detailed description of the Deep learning framework and dataset is presented. Experimental results and comparative performance of the proposed deep learning and Extreme learning classifiers are investigated and discussed in section 4. Finally, this study is concluded with the main prospects in section 4.

2. Related Work

Related work is explained in table 1

Table 1. Existing Approaches Review

Ref	Year	Aim	Approach	Models	Application	Dataset	Finding
[15]	2023	Stacked DL and AI-based wavelet design for coronavirus detection from chest X-rays.	Transfer learning-based modified ResNet50 model.	MobileNetV2, DenseNet121, ResNet50, VGG19, Xception, InceptionV3, and specialized models such as COVID-Net and Dark-COVIDNet	Domain Detection of Covids via State-of-the- art Learning Techniques COVID-19 in Chest X-Rays	Covid-19 Dataset	Models with ResNet50 perform the best.
[23]	2023	COVID-19 Detection in X-Ray Images Using Transfer Learning and DL Models.	Stacked and Wavelet DL architecture	VGG19, ResNet50, Xception, and DarkNet19	Detection	A publicly Small COVID-19 images dataset	Accuracy for the proposed model was 94.24% over 4 classes (viral pneumonia, COVID-19, normal, bacterial pneumonia), and 96.10% across 3 classes (pneumonia, COVID-19).
[5]	2022	To automate CXR analysis,	DL approaches	ResNet-50	COVID-19 cases detection	COV-PEN dataset	The suggested approach performs as well for expert

		thereby substantially lowering the time required for analysis.					radiologists, with a total precision of 100%, accuracy of 99.63%, an F1-score of 99.44%, a recall of 98.89%, and an AUC of 100%.
[8]	2022	To use a CNN to find COVID-19 in chest X-ray pictures.	NCA method	Efficientnetb0, Darknet53, and MobilenetV2 deep models	Chest X-rays for COVID-19 pneumonia differentiation from other viral pneumonia.	There are two groups of information on chest X-rays, COVID-19, viral pneumonia, and normal.	First data set: 99.05%, second dataset: 97.1%.
[3]	2021	To use a CNN to find COVID-19 in chest X-ray pictures.	An automatic DL classification method	CNN models; VGG19, VGG16, InceptionV3, MobileNetV2, ResNet50, ResNet101, NFNet EfficientNetB7, DenseNet, GoogLeNet. And AlexNet	Automated detection of the COVID-19 virus using chest X-rays.	A chest X-ray database	The most accurate (98%), out of all the deployed CNN models, at differentiating between COVID-19 and healthy chest X-rays.
[4]	2021	The purpose of this test is to identify cases of pneumonia due to COVID-19.	CNN	Pre-trained and customized DL models base on CNNs	Detection of covid must meet stringent clinical standards.	USNLM Montgomery County X-ray set, RSNA dataset, COVID-19	With the combination of datasets, the findings indicate a detection accuracy of 98.7%.

3. Materials and Methods

Material

The first dataset (Dataset-1) contains CXR (chest X-ray) pictures from three different classes: normal, COVID-19, and pneumonia. The dataset was obtained from the Figshare repos- itory on November 21, 2022. A total of 2250 CXR samples were obtained, with 750 from each class. The COVID-19 instances were mostly gathered from available sources that are updated on a regular basis.

Another dataset named COVIDx-V7A (Dataset-2) was used to assess the effectiveness of the proposed model. This dataset, which contains 15,999 CXR pictures from 15,122 patients from 51 nations, is the biggest open-access dataset accessible to date. The photos were gathered from five distinct data repositories and may be seen at "https://github.com/lindawangg/COVID-Net," which was retrieved on November 21, 2022.Specifies comprehensive requirements for the datasets under consideration, such as the number of photos in each class, image size, and

image format. In the first dataset, data imbalance is cited as a serious worry, which may have ramifications

To minimize biased performance estimates and assure the model's dependability, it is critical to resolve data imbalance in the dataset

Proposed Method

Steps for Analysis

Preprocessing of images

$$\mathbf{P} = \sum_{j=1}^{N} \overrightarrow{\propto} \boldsymbol{P_i ly_s P_i} \dots\dots\dots\dots\dots\dots (\mathbf{1})$$

$\boldsymbol{P_i}$ = Pixel Enhancement prediction

$$\text{Information gain} = 1 - \text{Entropy} \dots\dots\dots (2)$$

Step 1: Input x-ray image dataset with pre-processing and labels.

Step 2: Segmentation by k-mean optimization by this process given the efficient weight to pixel.

$$w_j^i = \begin{pmatrix} segmented & if\ clustering\ >\ noise \\ 0 & if\ noise\ =\ 0 \\ no\ segmented & otherwise \end{pmatrix} \dots (3)$$

Step 3: After segmentation finish go to efficient CNN using following activation function or fitness function.

$$d(L_i, L_j) = \sum_{i=1}^{M} \left(\theta_i X_{i,j} - \theta_i X_{i,j}\right) \dots\dots\dots\dots (4)$$

It finds the two-class distance and according to it finds activation space here L_i, L_j are the classes, W_i are the optimize weights as per the features.

Step 4: After finding the optimize weight. Apply LSTM-RNN

$$\partial^Z = \frac{(\partial^Z|^T . 1}{\sum_{i=1}^{M} (\partial^K|^C . 1} \dots\dots\dots\dots\dots\dots\dots\dots (5)$$

By equation (5) find the optimal features solution in The function of feature extraction is done by a second-generation CNN. It comprises three repeated stages of triplets of split, predict and update layers and a max pooling layer. Two features are extracted from each signal containing 2048 data points. The kernels used for convolution in the pair of predict and update layers in

LSTM-RNN: The preprocessed signal is fed to the first split layer where it is divided into an odd series and an even series. Downsampling the signal by two results in

Data compression is achieved by three max pooling

for the deep learning model's training and validation

space of

∂^Z then

Step 5:

$$\nabla = \max_k \partial^k \dots\dots\dots\dots\dots\dots\dots\dots\dots (6)$$

$$\mathrm{w} = argmax(\nabla) \dots\dots\dots\dots\dots\dots\dots\dots\dots (7)$$

By this find the maximize optimal features

Step 6: After optimizing the weights of the weighted feature learn by classifier.

$$L_N(.) = \sum_{i=1}^{N} C_N * \theta_N(.) \dots\dots\dots\dots\dots\dots (8)$$

$C_N(.)$ Boosting Classifier

C_N Number of weak classifiers

$\theta_N(.)$ Weight of features

After boosting all the possibilities send it to Bagging approach

$$B = \sum_{i=1}^{N} C_N(.) * \sum_{i=1}^{N} \theta_i \dots\dots\dots\dots\dots\dots (9)$$

$$L = \alpha C_N(.) + 1 - \alpha(\partial_K) \dots\dots\dots\dots\dots\dots (10)$$

By (9) use bagging and use (10) for combining both develop a classification model. Here α is the learning parameter α [0, 1]

Convolution Architecture: The advantages of CNN, second-generation wavelet transform and XG-BOOST are merged together to form a new classification technique. The feature extraction is performed by using the CNN with lifting scheme and classification is done using XG-BOOST. Thus, the better features can be found with an optimal tradeoff between computational speed, classification performance and memory space.

each stage are gaussian kernels each of size 1024x1, 512x1 and 256x1 respectively. A gaussian kernel is a general-purpose kernel commonly utilized in cases where there is no a-prior knowledge about the data. Irrespective of the signal being convoluted gaussian kernel works effectively.

the even series. Odd series is obtained by shifting and downsampling the signal. The learning is achieved by the split-predict-update loop.

layers. A max pooling layer is present after each trio of

split, predict and update layers. The max pooling layer is a 4X1 filter with a stride of four. The feature map generated from the final update layer is applied to XG-BOOST for classification.

The feature extraction is performed using the convolutional neural network with lifting scheme and classification is achieved using SVM. A second-generation CNN with XG-BOOST classifier can diagnose and distinguish between COPD and CHF with the two features extracted. The com- bination of second-generation CNN and XG-BOOST with linear kernel shows excellent performance in classification. The introduction of the lifting scheme can accelerate the speed of computation. Thus, the optimum feature can be extracted with better computational speed, classification performance, and memory space. Algorithm 2 summarizes the methodology of the Second-Generation CNN.

The architecture of RNNs also behaves as the fundamental network architecture for LSTM models. During the execution phase of RNN, a deep learning of hidden nodes receives the array input as X_f and produces the output sequence Y_t. This algorithm represents almost every temporal recursion, t, the learning algorithm of hidden units and retains the output of previous hidden cell, *ht*, and then adjusts its weight accordingly with the bias function for input layer, X_t, and the output of previous hidden cell was given as $h_t - l$ *, in the expanded architecture of Recurrent neural network, illustrated with the equation 1.

$$h_t = \sigma_h(W_{xh}x_t + W_{hh}h_{t-1} + b_h)$$

$$Y_t = \sigma_Y(W_{Yh}h_t + b_Y) \dots\dots\dots\dots\dots\dots (11)$$

whereas W_{xh} represents weight matrix connecting the input nodes phase, W_{hh} acts as weight factor between two successive hidden states *(h_t-land h_t)*, b_h was the hidden layer's skew component, and *O"h* resembles activation function hidden region. The outcome of overall system was described as following equation (2) W_{Yh} seemed to be the weighted sum through the hidden units towards its output nodes, *by* which provides the efficiency output of weighted vector, and *O"y* had this same output elements of bias vector.

The variables of these Recurrent neural network were learned and adjusted continuously using the back-propagation method by using equations (1) and (2). The deep learning model can even create a signal Y_t , for every iteration of time *t* , and indeed the final outcome, Y_r , has been the required anticipated performance for the following time unit , precisely $X_r+1 = Y_r$. Traditional RNNs struggle out from disappearing or incinerating the pattern within the development back propagation process, making them ineffective to understand the delay and form long duration information or expressing long-term correlations [81], despite their better capacity to re-

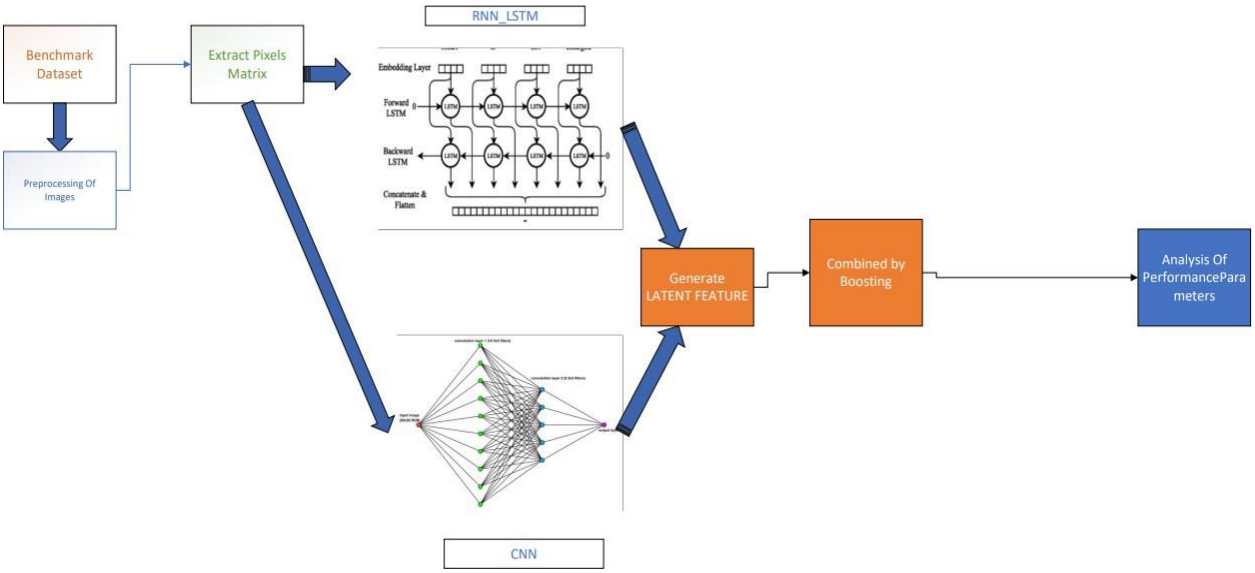

Fig 1. Proposed Method Flow Chart

ALGORITHM

INPUT: X_RAY IMAGE DATASET OUTPUT: PERFORMANCE PARAMETERS

1. **Input X-ray Images with label**
2. **Preprocess and enhance by eq (1)**
3. **Segmentation by eq (2) and eq (3)**
4. **Extract newly generated ∂_i vector of pixel images**
5. **After segmentation apply CNN with eq (4)**
6. **Optimize activation s function and find the optimize LSTM-RNN weight by eq (5) and get weights eq (6) and eq (7)**
7. **Learning by Boosting eq (8) and Bagging eq (9)**
8. **Make Classifier model eq (10) and analysis**
9. **Output Accuracy, Precision and other performance metrics**

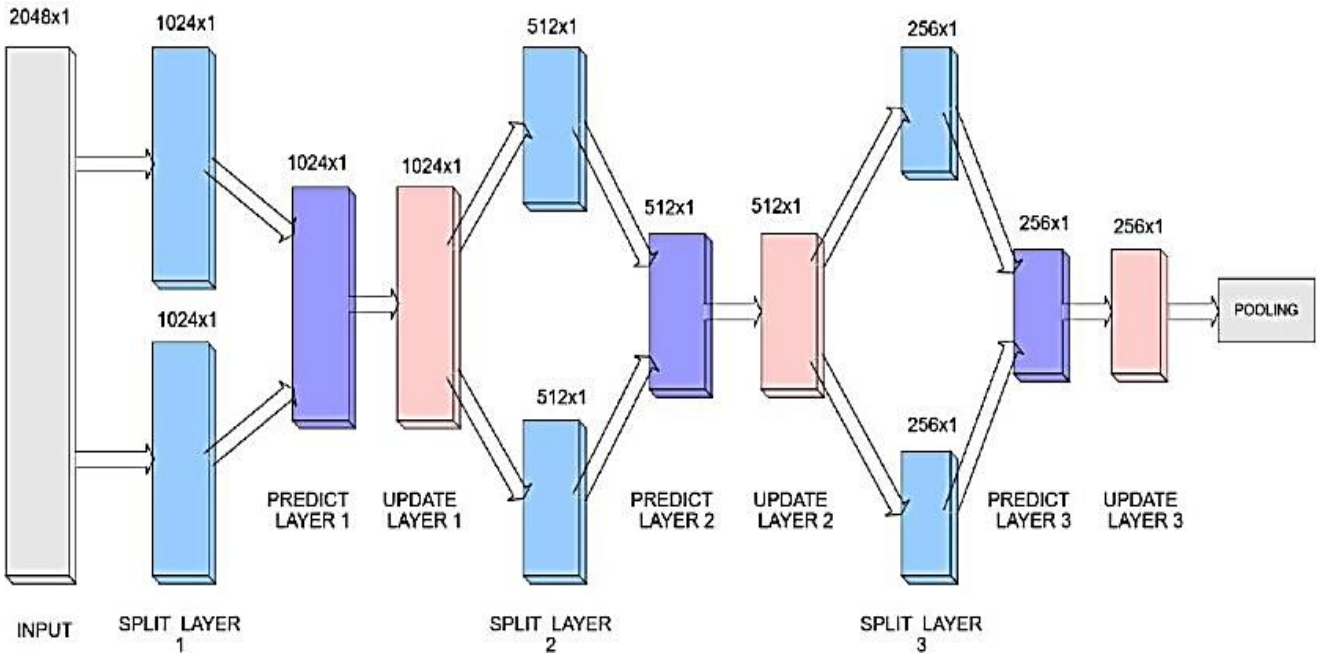

Fig 2. Convolution Architecture

-present multivariate time sequence issues. sequential problems that have long-term constraints, the LSTMs are said to perform effectively. Despite the fact that a number of conventional LSTM variations have been developed in the past years, a huge assessment of LSTM modifications demonstrates that neither of them considerably outperform the basic LSTM design [88]. As a result, the typical LSTM design has been used as part of such suggested topology in this research and therefore it is explained in the following subsection. The hidden units [89] act as a main difference among regular LSTM design and RNN layout. In LSTM layer, which has been exhibited in Fig. 3, was commonly described as the multiple hidden nodes of LSTM. The Memory unit in LSTM, is similar to the RNNs, and possesses a separate data

input, X_t, with an outcome phase h_t, for every periodic time, *t.* During the training process and also when adjusting characters to update the output of preceding cell, the convoluted unit considers the input and depends on the outcome of cell state, C_t , with the present cell state, C_t, and the preceding unit cell state, C_{t-1}'

4. Results and Analysis

Table 2 shows the experiment analysis of the proposed approach on several performance indicators from Dataset-1. The results of the 10-fold cross validation are shown. The average performance for accuracy, precision, sensitivity, specificity, and F1-score were 96.2646, 96.2097, 95.3675, 96.0639, and 96.5694, respectively. The 8th cross validation (98.333) was the most accurate, and the 1st cross validation (93.44) was the least accurate. In terms of precision, the 8^{th} cross validation (98.555) got the most accurate result, while the 2nd cross validation (95.3) got the least accurate precision result. In terms of sensitivity, the 8th cross validation (96.55) did the best, while the 9th cross validation produced the lowest number (93.44). Likewise, in terms of specificity, the 2^{nd} cross validation (97.56) achieved the highest specificity and the lowest one is obtained at the 9th fold. Yet, in terms of F1-score, the 8^{th} cross validation (98.55) achieved the most accurate F1 score, while the 4^{th} cross validation (94.55) achieved the lowest.

Table 3 shows the experiment analysis of the proposed approach on several performance indicators from Dataset-2. The results of the 10-fold cross validation are shown. The average performance for accuracy, precision, sensitivity, specificity, and F1-score were 98.037, 96.605, 95.766, 96.3066, and 96.1913, respectively. In terms of accuracy, the 6^{th} cross validation (99.55) was the most accurate as compared to the other validations. The third cross validation (98.55) yielded the most accurate result in terms of precision. In terms of sensitivity, 7^{th} cross validation (97.55) performed the best, whereas the others achieved significantly lower numbers. Similarly, the 8^{th} cross validation had the highest specificity (97.656). Nonetheless, the $3^{r\ d}$ cross validation (97.54) yielded the highest accurate F1-score when compared to the other validations.

Table 4 shows a comparison between the proposed approach experiment analysis and the existing approach experiment analysis for various performance metrics on Dataset-1 using different parameters. In terms of accuracy, precision, sensitivity, specificity, and F1-score, the proposed approach out- performs the methodological approaches, hence providing the highest quality to complete the operation. In terms of accuracy, the proposed method (96.26) outperforms the other methods followed by VGGNET-16, RESNET-50, and Capsule NET. In case of precision also, the proposed method (96.2097) outperforms the other methods followed by VGGNET-16, RESNET-50, and Capsule NET. The proposed technique outperformed with a 95.3675 sensitivity score, followed by Capsule NET, VGGNET-16, and RESNET-50. Similarly, the suggested technique (96.0639) surpassed RESNET-50, Capsule NET, and VGGNET-16 in terms of specificity. Yet, in terms of F1-score, the proposed method (96.5694) achieved the most accurate F1 score followed by VGGNET-16, RESNET-50, and Capsule NET.

Table 5 shows a comparison between the proposed approach experiment analysis and the existing approach experiment analysis for various performance metrics on Dataset-2 using different parameters. In terms of accuracy, precision, sensitivity, specificity, and F1-score, the proposed approach out- performs the methodological approaches, hence providing the highest quality to complete the operation. In terms of accuracy, the proposed method (95.185) outperforms the other methods followed by VGGNET-16, Capsule NET, and RESNET-50. In case of precision also, the proposed method (93.27995) outperforms the other methods followed by VGGNET-16, RESNET-50, and Capsule NET. The proposed technique outperformed with a 92.97125 sensitivity score, followed by Capsule NET, VGGNET-16, and RESNET-50.

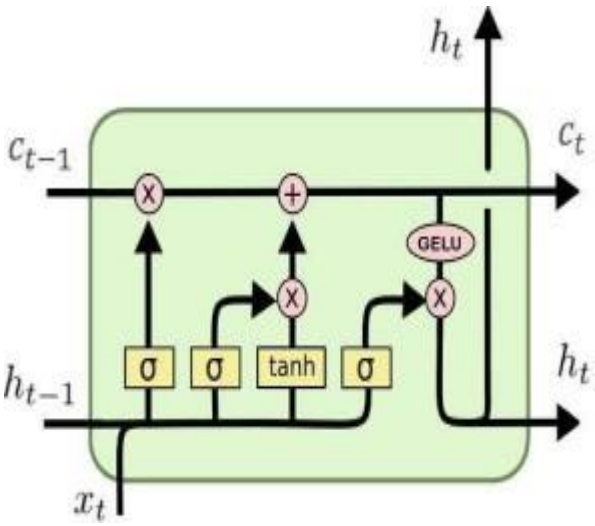

Fig 3. LSTM Architecture

Similarly, the suggested technique (91.90398333) surpassed in terms of specificity. Yet, in terms of F1-score, the proposed method (92.488233) achieved the most accurate F1 score followed by RESNET-50, VGGNET-16, and Capsule NET. Table 6 compares the proposed method to previous current investigations. The proposal employing BILSTM-ATTEN outperformed other current literature investigations, as shown in the table, with binary and multiclass values of 99.78 and 96.45, respectively.

Table 2. Proposed Approach Experiment Analysis on Different Performance Metrics on Dataset-1

CROSS VALIDATION	ACCURACY	PRECISION	SENSITIVITY	SPECIFICITY	F1-SCORE
1	93.44	96.44	95.4	96.45	96.54
2	95.445	95.3	96.44	97.56	95.434
3	96.44	94.345	95.43	95.44	97.54
4	96	97.444	94.55	96.44	94.55
5	96.44	96.344	96.55	97.44	96.77
6	95.22	96.455	95.43	96.43	95.56
7	97.444	95.33	95.44	95.44	97.65
8	98.333	98.555	96.55	96.554	98.55
9	96.44	96.44	94.44	93.44	96.55
10	97.444	95.444	93.445	95.445	96.55
Average	**96.2646**	**96.2097**	**95.3675**	**96.0639**	**96.5694**

Table 3. Proposed Approach Experiment Analysis on Different Performance Metrics on Dataset-2

CROSS VALIDATION	ACCURACY	PRECISION	SENSITIVITY	SPECIFICITY	F1-SCORE
1	97.54	97.44	95.55	96.44	96.44
2	97.4	96.44	94.55	96.55	95.44
3	97.66	98.55	96.44	95.44	97.54
4	98.555	96.44	95.43	97.44	96.54
5	98.55	95.44	95.43	96.54	93.44
6	99.55	97.55	96.5	94.55	96.54
7	96.55	96.55	97.55	96.4	97.44
8	98.45	94.55	94.44	97.656	96.44
9	97.55	97.54	95.44	95.5	96.433
10	98.565	95.55	96.33	96.55	95.66
Average	**98.037**	**96.605**	**95.766**	**96.3066**	**96.1913**

Table 4. Comparison Of Proposed and Existing Approach Experiment Analysis on Different Performance Metrics on Dataset-1

APPROACHES	ACCURACY	PRECISION	SENSITIVITY	SPECIFICITY	F1-SCORE
RESNET-50	93.45	91.34	90.23	92.45	91.34
VGGNET-16	95.23	94.34	92.34	90.12	92.45
Capsule NET	93.14	91.23	93.23	91.56	90.12
PROPOSED	**96.26**	**96.2097**	**95.3675**	**96.0639**	**96.5694**

Table 5. Comparison of Proposed and Existing Approach Experiment Analysis on Different Performance Metrics on Dataset-2

APPROACHES	ACCURACY	PRECISION	SENSITIVITY	SPECIFICITY	F1-SCORE
RESNET-50	94.23	92.33	91.32	92	93.22
VGGNET-16	96.13	94.34	92.34	90.12	92.45
Capsule NET	96.12	91.23	93.23	91.56	90.12
PRO-	**95.185**	**93.27995**	**92.97125**	**91.90398333**	**92.48823333**

Soumya Ranjan Nayak et al. [25] employed the LW-CORONet approach to achieve the second-best binary and multiclass values (i.e., 98.56 and 94.44). Narin et al. [19] used ResNet-50 to place third in binary and multiclass values (i.e.,90.2 and 87.02). While some prior studies are inapplicable to binary and

multiclass classification.

Table 6. Comparison of Proposed and Existing Research Experiment Analysis on Different Performance Metrics on Binary and Multiclass

AUTHORS	METHODS	BINARY	MULTI- CLASS
Hemdan et al. [1]	**COVIDX-Net**	90.2	87.02
Narin et al. [24]	**ResNet-50**	98.12	94.34
Ozturk et al. [25]	**DarkCovidNet**	98	91.4
Ucar and Korkmaz [26]	**Bayes-SqueezeNet**	NA	93.44
Rahimzadeh and Attar [27]	**Xception and ResNet50V2**	NA	NA
To ˘gaçar et al. [28]	**SqueezeNet and MobileNetV2**	NA	NA
Nayak et al. [29]	**ResNet-34**	98.33	NA
Toramana et al. [30]	**CapsNet**	NA	84.22
Soumya Ranjan Nayak et.al. [23]	**LW-CORONet**	98.56	94.44
PROPOSED	**BILSTM-ATTEN**	99.78	96.45

Figure 2 represents the segmented images with original and predicted masks. Image masking is a very helpful method for non-destructively editing visual images. With image masking, one may conceal, reveal or hide some parts of the image and reveal parts offering greater versatility in editing the images. Figure above depicts the original and predicted masks of the chest region providing visual information on the process. Figure 3 depicts the confusion matrix of the proposed multiclass technique based on multiple datasets, including normal, COVID-19, Lung opacity, and viral pneumonia cases. The graph illustrates the exceptional performance of the proposed model on each image type. The model performed well across all four classes, with Pneumonia (131) having the lowest proportion of misclassified instances compared to class size.

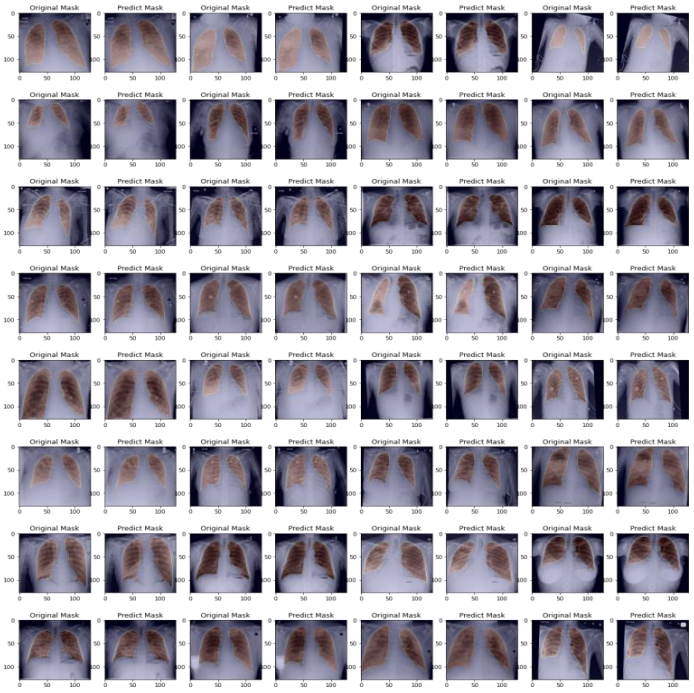

Fig 4. Segmented Images with original and predicted mask

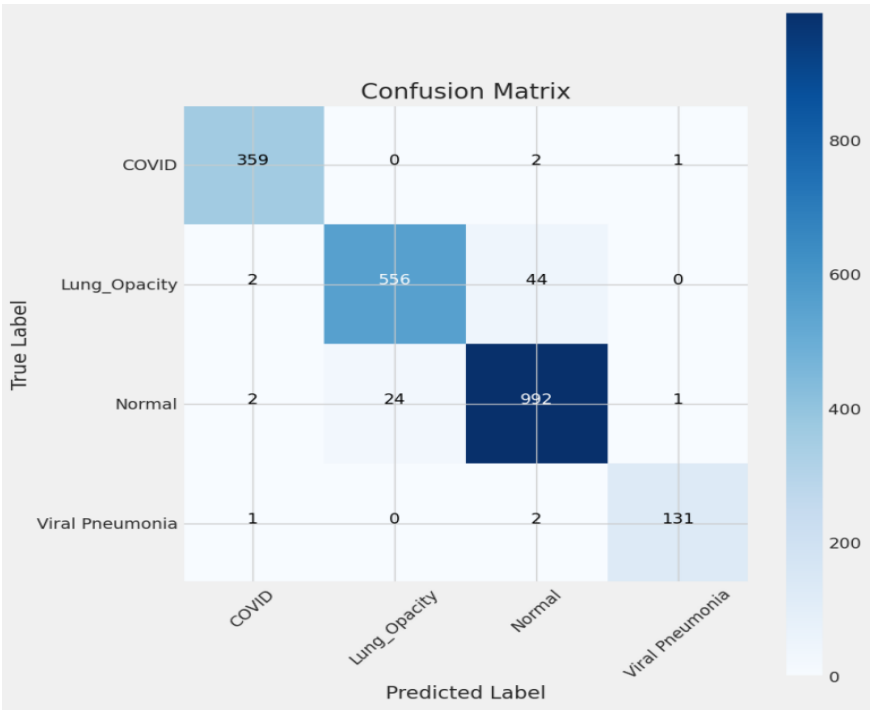

Fig 5. Confusion matrix of proposed approach on multiclass

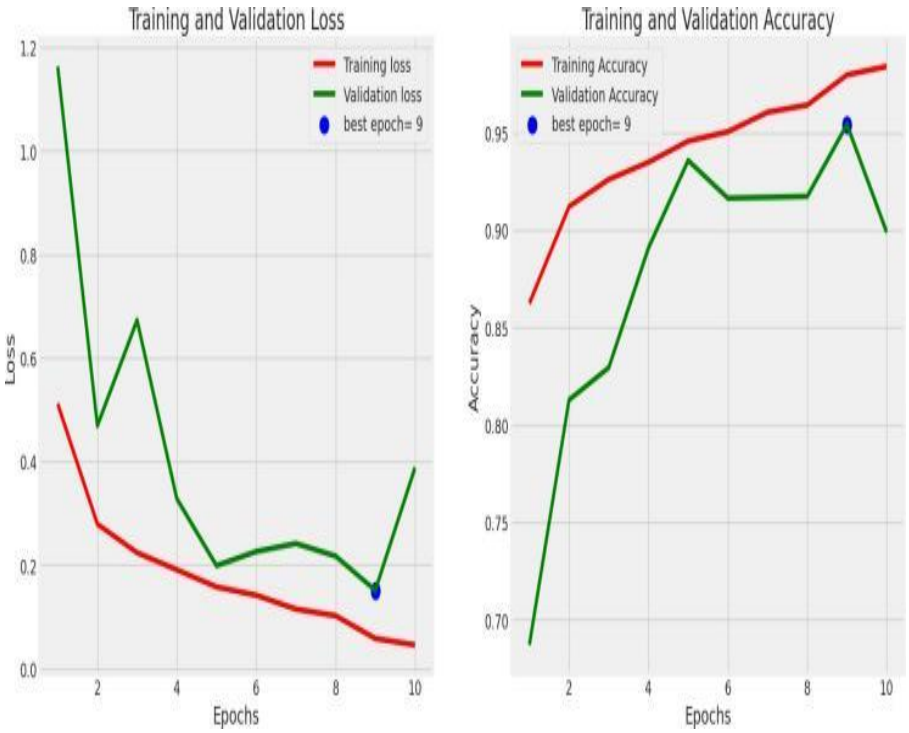

Fig 6. Epoch wise accuracy analysis of proposed approach on multiclass

Figure 4 shows the epoch wise accuracy analysis of proposed approach on multiclass. Figure 3 left analysis represents the training and validation loss values showing a falling trend. At the 2nd epoch, the validation loss is 0.5 whereas the training loss obtained is around 0.3. At the 4th epoch, the validation loss is around 0.36 whereas the training loss obtained is 0.2 The best epoch value is obtained in between 8th and 10th epoch around 0.15 as shown in the graph. On the other hand, the right portion of the figure represents the training and validation accuracy values showing a rising trend. At the 2nd epoch, the validation accuracy is 0.82 whereas the training accuracy obtained is around 0.92. At the 4th epoch, the validation accuracy is around 0.89 whereas the training accuracy obtained is 0.93. The best epoch value is obtained in between 8thand 10th epoch (0.95) as shown in the graph

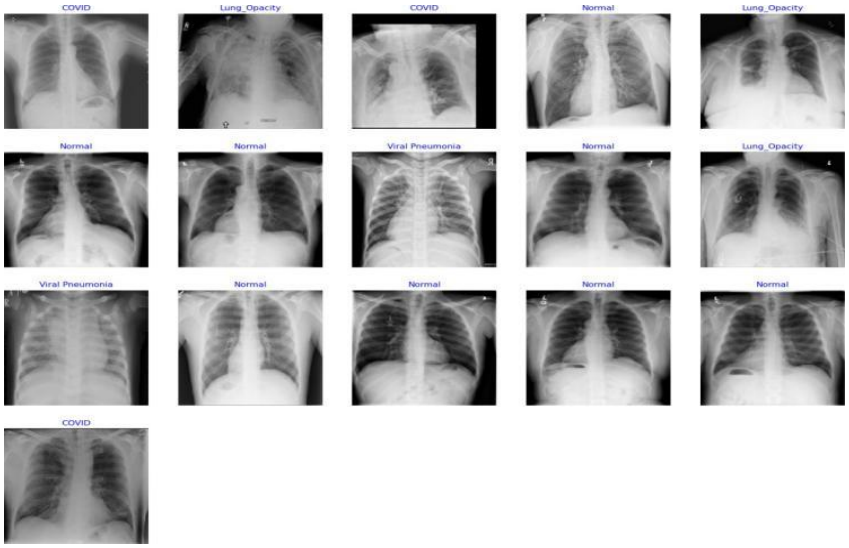

.

Fig 7. Predicted images of proposed approach on multiclass

Fig 5 shows the predicted images using the proposed approach on multiclass. The figure above shows several examples of visual perspectives for each of the classes i.e., normal, COVID-19, Lung opacity, and viral pneumonia cases.

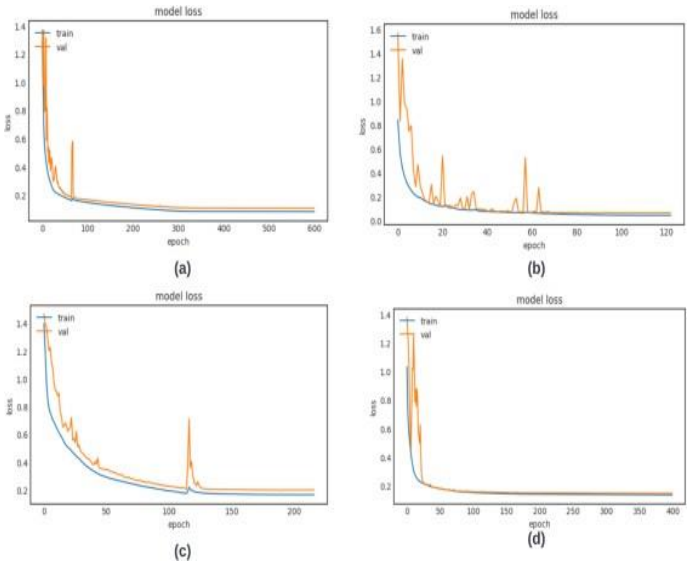

Fig 8. Loss graph of proposed model on (a) MC (b) Shenzhen (c) NIH datasets (d)CT-Scan datasets

Conclusion

The CONLST- BOOST (proposed model) in the paper is designed to accurately and efficiently detect COVID-19 infection from chest radiography (CXR) images. It consists of only five learnable layers, making it lightweight and requiring low computational power and memory space. The model was extensively validated using two publicly available CXR datasets, and the effect of hyperparameters was analyzed to optimize performance. The CONLST- BOOST (proposed model) outperformed pre-trained CNN models and existing approaches in both multi-class and binary classification scenarios. According to the findings of the research, the suggested CONLST- BOOST (proposed model) acquired a high level of accuracy while identifying COVID-19 infection using CXR images. The accuracy of classification that was achieved for multi-class and binary classification instances, respectively, was 98.67% on Dataset-1 and 99.00% on Dataset-2. On Dataset-2, the respective figures were 95.67% and 96.25%. These findings performed much better than the contemporaneous pre-trained CNN models as well as the state-of-the-art models that were utilized for comparison. The experiments also showed that the performance of the proposed model was affected by different hyper parameters such as optimization techniques, batch size, and learning rate. By tuning these hyperparameters, the researchers were able to achieve the best detection performance. Overall, the proposed model was found to be effective, lightweight, and suitable for real- time COVID-19 diagnosis

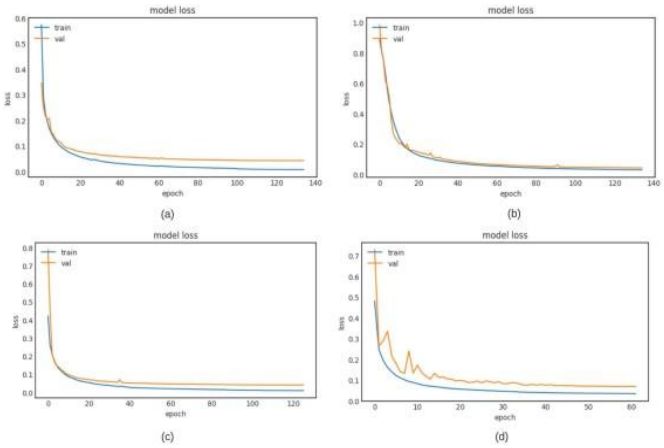

Fig 9. Dice coefficient loss graph for the EfficientUNet trained and tested on (a)Shenzhen (b) MC (c) Combined (Shenzhen+MC) (d) Trained on Shenzhen and testedon MC dataset

References

[1] E. E. D. Hemdan, M. A. Shouman, and M. E. Karar.G. Jain, D. Mittal, D. Thakur, and M. K. Mittal, "A deep learning approach to detect Covid-19 coronavirus with X-Ray images," *Biocybernetics and biomedical engineering*, vol. 40, no. 4, pp. 1391–1405, 2020.

[2] R. Jain, M. Gupta, S. Taneja, and D. J. Hemanth, "Deep learning- based detection and analysis of COVID-19 on chest X-ray images," *Applied Intelligence*, vol. 51, pp. 1690–1700, 2021.

[3] M. Markom, M. Taha, A. Adom, A. Sukor, A. Nasir, H. Yazid. Markom, and A. M, "A review: deep learning classification performance of normal and COVID-19 chest X-ray images," *In Journal of Physics: Conference Series*, vol. 2071, no. 1, pp. 12 003–12 003, 2021.

[4] M. E. Sahin, "Deep learning-based approach for detecting COVID-19 in chest X-rays," *Biomedical Signal Processing and Control*, vol. 78, pp. 103 977–103 977, 2022.

[5] A. Bashar, G. B. Latif, G. Brahim, N. Mohammad, and J. Alghazo, "COVID-19 pneumonia detection using optimized deep learning techniques," *Diagnostics*, vol. 11, no. 11, 1972.

[6] T. Jung and N. Vij, "Early diagnosis and real-time monitoring of regional lung function changes to prevent chronic obstructive pulmonary disease progression to severe emphysema," *Journal of Clinical Medicine*, vol. 10, no. 24, pp. 5811–5811, 2021.

[7] A. Sharma, K. Singh, and D. Koundal, "A novel fusion-based convolutional neural network approach for classification of COVID-19 from chest X-ray images," *Biomedical Signal Processing and Control*, vol. 77, pp. 103 778–103 778, 2022.

[8] S. Asif, Y. Wenhui, H. Jin, and S. Jinhai, "Classification of COVID-19 from chest X-ray images using deep convolutional neural network," *2020 IEEE 6th international conference on computer and communications (ICCC)*, pp. 426–433, 2020.

[9] S. Mahajan, Raina, X. Gao, and A. K. Pandit, "COVID-19 detection using hybrid deep learning model in chest x-rays images," *Concurrency and Computation: Practice and Experience*, vol. 34, no. 5, pp. 6747– 6747, 2022.

[10] E. E. Hemdan, M. Shouman, and M. E. Karar,

2020.

[11] A. Narin, C. Kaya, and Z. Pamuk, "Automatic detection of coronavirus disease (covid-19) using x-ray images and deep convolutional neural networks," *Pattern Analysis and Applications*, vol. 24, pp. 1207–1220, 2021.

[12] S. Chakraborty, B. Murali, and A. K. Mitra, "An efficient deep learning model to detect COVID-19 using chest X-ray images," *International Journal of Environmental Research and Public Health*, vol. 19, no. 4, 2013.

[13] N. Brandi, Ciccarese, M. Rimondi, C. Balacchi, C. Modolon, Sportoletti, and R. Golfieri, "An imaging overview of COVID-19 ards in ICU patients and its complications: a pictorial review," *Diagnostics*, vol. 12, no. 4, pp. 846–846, 2022.

[14] S. Agrawal, V. Honnakasturi, M. Nara, and N. Patil, "Utilizing Deep Learning Models and Transfer Learning for COVID-19 Detection from X-Ray Images," *SN Computer Science*, vol. 4, no. 4, pp. 326–326, 2023.

[15] I. Apostolopoulos and T. A. Mpesiana, pp. 635–640, 2020.

[16] S. Vj, "Deep learning algorithm for COVID-19 classification using chest X-ray images," *Computational and Mathematical Methods in Medicine*, 2021.

[17] M. Loey, S. El-Sappagh, and S. Mirjalili, "Bayesian-based optimized deep learning model to detect COVID-19 patients using chest X-ray image data," *Computers in Biology and Medicine*, vol. 142, pp. 105 213– 105 213, 2022.